Self-assembling as regular nanoparticles dramatically minimizes photobleaching of tumor-targeted GFP

Ugutz Unzueta [a,b,c, ‡, *] Mònica Roldán [d,h ‡,] Mireia Pesarrodona [b,c,e $,] Raul Benitez [g,h]

Alejandro Sánchez-Chardi [f], Oscar Conchillo-Solé [e], Ramón Mangues [a, b], Antonio

Villaverde [b,c,e *] and Esther Vázquez [b,c,e *]

[a] Institut d'Investigacions Biomèdiques Sant Pau, Hospital de la Santa Creu i Sant Pau, 08025 Barcelona, Spain

[b] CIBER de Bioingeniería, Biomateriales y Nanomedicina (CIBER-BBN), C/ Monforte de Lemos 3-5, 28029 Madrid, Spain

[c] Departament de Genètica i de Microbiologia, Universitat Autònoma de Barcelona, Bellaterra, 08193 Barcelona, Spain

[d] Unitat de Microscòpia Confocal. Servei d'Anatomia Patològica, Institut Pediàtric de Malalties Rares (IPER), Hospital Sant Joan de Déu, Esplugues de Llobregat, Barcelona, España

[e] Institut de Biotecnologia i de Biomedicina, Universitat Autònoma de Barcelona, Bellaterra, 08193 Barcelona, Spain

[f] Departament de Biologia Evolutiva, Ecologia i Ciències Ambientals, Facultat de Biologia, Universitat de Barcelona, Av. Diagonal 643, 08028 Barcelona, Spain.

[g] Biomedical Engineering Research Center and Automatic Control Department, Universitat Politècnica de Catalunya, Av. Eduard Maristany 16, 08019 Barcelona, Spain.

[h] Institut de Recerca Sant Joan de Déu, Santa Rosa 39-57, 08950 Esplugues de Llobregat, Spain

[ǂ] Equally contributed

[$] Present address: Institute for Research in Biomedicine (IRB Barcelona), The Barcelona Institute of Science and Technology, Barcelona 08028, Spain.

[*] Corresponding authors.

UU: UUnzueta@santpau.cat , AV: antoni.villaverde@uab.es ,

EV: esther.vazquez@uab.es

ABSTRACT

Fluorescent proteins are useful imaging and theranostic agents, but their potential superiority over alternative dyes is weakened by substantial photobleaching under irradiation. Enhancing protein photostability has been attempted through diverse strategies, with irregular results and limited applicability. In this context, we wondered if the controlled oligomerization of Green Fluorescent Protein (GFP) as nanoscale supramolecular complexes could stabilize the fluorophore through the newly formed protein-protein contacts, and thus, enhance its global photostability. For that, we have here analyzed the photobleaching profile of several GFP versions, engineered to self-assemble as tumor-homing nanoparticles with different targeting, size and structural stability. This has been done under prolonged irradiation in confocal laser scanning microscopy and by small-angle X-ray scattering. The results show that the oligomerization of GFP at the nanoscale enhances, by more than seven-fold, the stability of fluorescence emission. Interestingly, GFP nanoparticles are much more resistant to X-ray damage than the building block counterparts, indicating that the gained photostability is linked to enhanced structural resistance to radiation. Therefore, the controlled oligomerization of self-assembling fluorescent proteins as protein nanoparticles is a simple, versatile and powerful method to enhance their photostability for uses in precision imaging and therapy.

KEYWORDS

Nanoparticles; fluorescent proteins; photostability; self-assembling; tumor targeting

1. INTRODUCTION

Among the catalogue of fluorescent proteins with applicability in biomedicine [1], GFP has been widespread explored for therapeutic uses *in vitro* and *in vivo*, including full body and tissue imaging. In oncology, lighting up tumors and metastatic foci is appealing for image-assisted surgery [2, 3], an application for which GFP has been specifically adapted by the incorporation of tumor-homing peptides [4-8]. Although GFP (and other fluorescent proteins) presents advantages over fluorescent dyes and quantum dots [5], photobleaching, namely the fading of fluorescent emission during light excitation [9], impairs the optical detection of tumoral tissues at low emission levels such as those expected in micrometastasis [10-12]. High-quality imaging and quantitative analyses of fluorescence signals demand robust fluorescence emission [13]. In this context, different approaches have been explored to improve the photostability of fluorescent proteins [14-16], including directed molecular evolution and protein engineering [17], association with metals [18], or manipulation of cell culture media composition [16, 19].

In recent studies, we have engineered peptide-tagged recombinant GFP versions, that self-assemble as nanoparticles (NPs) of sizes ranging from 12 nm to 60 nm [20-22], to successfully deliver small molecular weight drugs [23] and human pro-apoptotic factors [24] to metastatic cancer stem cells, in colorectal cancer animal models. The biodistribution of these materials, as determined by fluorescence detection, is highly specific and it fulfills the high standards required for both, drug delivery and imaging [10]. These proteins are internalized in target cells but not in normal organs. Then, the main tumor and metastatic foci selectively become highly fluorescent [10]. In this context, we wondered if the controlled self-assembling of GFP as regular nanoscale oligomers, sustained by the novo formed protein-protein contacts, might increase the

photostability of the protein, making it more suitable for theranostics than the standard unassembled forms. If so, protein engineering aimed to promote the formation of nanoscale supramolecular complexes could be a versatile and promising approach to reduce photobleaching of protein dyes. In this study, we have examined several tumor-homing GFP versions that spontaneously self-assemble as protein-only nanoparticles, with different size and structural stability, regarding their resistance to radiation stress.

The comparison of GFP-based NPs with the unassembled versions of the respective forming protein building blocks (BBs) has revealed that the formation of macromolecular complexes is a powerful and versatile approach to enhance phostostability and structural stability of protein imaging tools for theranostics.

2. MATERIALS AND METHODS

2.1 Protein design, production and purification

The synthetic genes encoding modular proteins (GFP-H6, T22-GFP-H6 and A5-GFP-H6) have been designed in-house and were provided by Geneart (ThermoFisher) cloned into pET22b (Novagen). Gene encoding for R9-GFP-H6 modular protein was produced in-house by directed mutagenesis and cloned into pET21b (Novagen). T22 (MRRWCYRKCYKGYCYRKCR), R9 (MRRRRRRRRR) and A5 (MRLVSYNGIIFFLK) are amino terminal peptide tags that act as tumour targeting agents, binding CXCR4 (T22 and R9, [10, 21]) and CD44 (A5, [25]) cell surface proteins respectively (supplementary data 1). Being cationic, they also promote self-assembling of the fusion protein as nanoparticles. All recombinant vectors were transformed and encoding proteins produced in *Escherichia coli* BL21 (Novagen) for A5-GFP-H6 and GFP-H6, Origami B (Novagen) for T22-GFP-H6 and Rosetta (Novagen) for R9-GFP-H6 upon addition of 0.1mM isopropyl β-D-1-thiogalactopyranoside (IPTG) overnight at 16ºC for A5-GFP-H6, at 20ºC for T22-GFP-H6 and GFP-H6 and at 25ºC for R9-GFP-H6. Cell pellets were then harvested by centrifugation (10 min at 5000 *g*) and resuspended in wash buffer (20 mM Tris, 500 mM NaCl, 10 mM imidazole; pH8) in presence of protease inhibitors (Complete EDTA free, Roche) for further purification. Cell disruption was performed at 1200 psi in a French Press (Thermo) and protein containing supernatants separated by centrifugation (45 min at 20000 *g*) for immobilized metal affinity chromatography (IMAC) purification in an Äkta pure system (GE Healthcare), using Hitrap Chelating HP columns (GE Healthcare). Proteins were eluted by a linear gradient of elution buffer (20mM Tris, 500 mM NaCl, 500 mM imidazole; pH 8) and purified proteins dialyzed against carbonate buffer (166 mM $NaCO_3H$; pH 8) for GFP-H6 and A5-GFP-H6, carbonate with salt buffer (166 mM $NaCO_3H$, 333 mM NaCl; pH

8) for T22-GFP-H6 and Tris dextrose buffer (20 mMTris + 5 % dextrose; pH 8) for R9-GFP-H6. Purified protein purity and identity was then analyzed by SDS-PAGE electrophoresis and further Western-blot immunodetection using anti-His monoclonal antibodies (Santa Cruz Biotechnology), and protein integrity determined by MALDI-TOF mass spectrometry (Bruker). Finally, protein concentration was determined by Bradford's assay. The self-assembling proteins T22-GFP-H6, A5-GFP-H6 and R9-GFP-H6 were found as NPs after purification. Protein building blocks (BBs) were obtained from NPs by disassembling upon addition of sodium dodecyl sulphate (SDS) to 0.1 % for 1 h. NPs and BBs for SAXS analysis of T22-GFP-H6 and A5-GFP-H6 were isolated using a Size-exclusion chromatography with a Superdex 200 Increase 10/300 GL column.

2.2 Dynamic Light Scattering (DLS)

Volume size distribution of self-assembled protein nanoparticles and SDS-mediated disassembled BBs were analyzed by DLS at 633 nm in a Zetasizer nano (Malvern Instruments). All samples were analyzed in triplicate at the same concentration (1mg/mL) and pH (pH=8) to avoid any concentration of pH-dependent variations.

2.3 Size Exclusion Chromatography (SEC)

Hydrodynamic size distribution of self-assembled protein nanoparticles was determined by size exclusion chromatography upon injection of 200ug protein sample in a Superdex 200 increase 10/300GL column (GE Healthcare) using an Äkta purifier system (GE Healthcare). Samples were run in their respective buffers supplemented with 0.1mM ZnCl2 to avoid losing nanoparticles coordinating divalent cations.

2.4 Fluorescence emission

Specific fluorescence emission was measured at 510 nm in a Varian Cary Eclipse Fluorescence spectrophotometer (Agilent Technologies) upon excitation at 488 nm, and relative fluorescence percentages were determined and related to control GFP-H6 protein. GFP-H6 protein showed a specific fluorescence of 840 fluorescence units mg/mL when measured in its respective buffer in a 1cm light path quartz cuvette and the detector was set at medium voltage and excitation and emission slits were set at 5 nm. All fluorescent data were measured at the same moment to avoid device-age related variances and were further normalized by molar concentration for comparison purposes.

2.5 Electron Microscopy (EM)

Size and shape of NPs were determined by EM at nearly native state with two rapid techniques and observed with high resolution electron microscopes [26]. Drops of 3 µL of NPs at 0.25 mg/mL were directly deposited on silicon wafers (Ted Pella Inc.) for 1 min, excess of liquid blotted with filter paper, air dried, and immediately observed without coating with a high resolution in-lens secondary electron detector in a field emission scanning electron microscope (FESEM) Zeiss Merlin (Zeiss) operating at 1 kV. For negative staining, drops of 3 µL of the same three samples were directly deposited on 200 mesh carbon-coated copper grids (Electron Microscopy Sciences) for 30 sec, excess blotted with filter paper, contrasted with 3 µL of 1 % uranyl acetate (Polysciences Inc.) for 1 min, blotted again and observed in a transmission electron microscope (TEM) Jeol 1400 (Jeol Ltd.) working at 80 kV and equipped with a GatanOrius SC200 CCD camera (Gatan Inc.) [26]. For each sample and technique, representative images of different fields were captured at high magnifications (from 100,000 x to 600,000 x).

2.6 Confocal Laser Scanning Microscopy (CLSM) and photobleaching measurements

Photobleaching measurements were performed with a Leica TCS SP8 STED 3 x (Leica Microsystems) using a Plan-Apochromatic 63 x objective (NA 1.4, oil). GFP-based structures were illuminated with a 20 mW argon laser 488 nm at a 20 % AOTF output and detected on a 500 to 550 nm spectral bandwidth. The laser illumination occurred without intermittence and each measurement was repeated at least four times using the same settings for all samples. Fluorescence intensity image size was fixed to 512 by 512 pixels with 12 bits of dynamic range, and the confocal pinhole was 2 AU diameter. For a 1600-Hz line scan rate, the total time between frames was 337 msec for 5 min. In the study area, 4 ROIs of 30 μm^2 were selected to show the MFI in the region in relation to time. All NPs and BBs samples were compared at the same molar concentration and pH in order to avoid any concentration or pH-dependent variations. Data from all studies were analysed using the LAS X software (Leica Microsystems).

2.7 Small-Angle X-ray Scattering (SAXS)

Radiation damage to protein samples was measured by evaluating progressive changes in SAXS profiles after multiple frames at 1-2 sec of exposure at 12.4 keV (λ = 1 Å) without attenuation recorded in the non-crystalline diffraction (NCD) beamline at ALBA synchrotron Light Source (Cerdanyola del Valles, Spain) using an imXPAD-S1400 photon-counting detector (imXPAD) placed at 5.9 m from the sample. Samples were measured in a Teflon cell with 25 μm thickness mica windows and 3 mm path length and radiation damage data was analysed by Microsoft Excel software (Microsoft).

2.8 Molecular modelling

Models were constructed as presented elsewhere [20]. Interface residues were determined by selecting those residues exposed to the surface of the protein in the monomer which surface accessibility changes in the NP. Those residues with 40 % or more surface accessibility were considered exposed as recommended in Haddock procedures [27]. Surface accessibility was calculated using the Naccess [28] program.

2.9 Statistical methods

Data were tested for normality and homogeneity of variances with Shapiro-Wilk and Levene tests, respectively. Confocal microscopy measurements are expressed as mean and standard error ($\overline{x}$ ± SE) and have been represented using SigmaPlot 10.0 software. Pairwise comparisons between protein groups were determined by paired t-tests also using SigmaPlot 10.0, and significant differences were assumed at $p<0.05$.

Pixelwise analysis of fluorescent decay has been done over 12-bit grayscale images of size 512x512 pixels with a physical pixel size of 0.181μm. From each experiment, samples of 525 pixels from a regular grid were fitted against one-, two- and stretched exponential time decay models to their pixel intensity. A two-exponential model [illegible] was selected using SSE and adjusted R-squared as goodness-of-fit parameters. From the fitted function, we obtained the Full Duration at Half Maximum (FDHM) as the time at which the fluorescence intensity decreased half of its initial amplitude. Differences in decay stability were then characterized using the distribution of FDHM among conditions. The comparison of the FDHM between parental GFP-H6 and NPs was found to be statistically significative in all cases ($p<0.001$, two-sided Wilcoxon rank sum test). A non-parametric test was applied since the samples were not normally distributed

($p<0.001$, Kolmogorov-Smirnov test). Similarly, comparison between each NPs and their respective SDS-mediated BBs was found to be statistically significative ($p<0.001$, two-sided Wilcoxon rank sum test).

3. RESULTS

GFP-H6 is a fluorescent fusion protein that remains unassembled, sizing around 5-6 nm (Figure 1 A), compatible with the occurrence of the dimer, the most common form of recombinant GFP [29, 30]. T22-GFP-H6, A5-GFP-H6 and R9-GFP-H6 are modular GFP-H6 derivatives that spontaneously self-assemble, upon purification, as regular NPs of sizes ranging from 12 nm (T22-GFP-H6) to 56 nm (A5-GFP-H6) (Figure 1A, B, C). They only differ in the amino acid sequence of the amino terminal peptide, which is highly cationic in the case of T22 and R9, and moderately cationic in the case of A5. These three peptides are completely unrelated in sequence and in source [10, 21, 25]. When treated with 0.1 % SDS, NPs disassembled as BBs of sizes comparable to that of the parental GFP-H6 (Figure 1A), with exception of R9-GFP-H6. This protein was not completely disassembled and remained partially organized as supramolecular structures, sizing 9 nm (Figure 1A), probably because of the high cationic load of the N-terminal peptide. All the tested modular proteins resulted fluorescent as NPs and as SDS-released BBs, allowing the exploration of their photostability under radiation stresses.The specific emission intensities were comparable to that of the parental GFP-H6 (Figure 1 A), being the fluorescence of the protein materials lower, in any case, than that of the unassembled GFP-H6. This fact excluded a potential enhancement of the fluorescence mediated by intermolecular protein-protein contacts in the NPs, which might interfere with photostability analyses. All NPs were also structurally stable and similarly fluorescent in a range of different physiological pH values, showing only low fluorescence reduction and moderate particles aggregation (only for A5-GFP-H6 NPs) at pH=6.5, the lowest expected pH for a physiological media (Supplementary Figure 1).

In the first step, solutions of GFP NPs were irradiated with a 20 mW argon laser at 488 nm, under a confocal microscope, to evaluate photobleaching of nanostructured GFP and

to compare the differential rate of fluorescence extinction of NPs, SDS-released BBs and parental control GFP-H6. As observed (Figure 2A), the rate of fluorescence decay was much slower in all NPs than in their respective SDS-generated BBs, which occurred at values comparable to those of control GFP-H6. When comparing to the parental GFP-H6, the photostability of GFP was generically enhanced in all oligomers by factors ranging from 2.5 to 7.7 (Table 1). However, when comparing to the SDS-generated BBs, R9-GFP-H6 NPs showed only a 2-fold factor of improved stability (Table 1, Figure 2A), fitting with the fact that the true BBs of this protein were not obtained. The increased photostability of the nanostructured forms of GFP was fully supported by the longer time periods required to reach both 50 % and 75 % of fluorescence reduction, compared to SDS-generated BBs, with statistically significant differences (Figure 2B). At that point and to exclude any protocol-related protein mixing problems, BBs and NPs of the model T22-GFP-H6, immobilized in polyacrylamide, were also analyzed, rendering results that fully validated our previous data (Supplementary Figure 2). Also, the impact of divalent cation that coordinate the assembling of NPs or the presence of SDS over the photostability of the samples was discarded by comparing EDTA-generated BBs (in which divalent cations have been removed by EDTA and no SDS was present) with SDS-generated BBs (which still contained divalent cations and SDS was also present). In this context, no significant differences were observed with control GFP-H6 (Supplementary Figure 3).

Then, in order to further study the fluorescence decay of our protein samples, pixel intensity data were fitted against different exponential decay models, including single exponential (a*exp(-b*t)), stretched exponential (a*exp(-b*x^c)) or double exponential (a*exp(-b*x)+c*exp(-d*x)+e), being the double exponential decay the one better describing the fluorescence extinction process (Figure 3A). At this point, and following

the selected decay model, pixelwise analysis of Full Duration at Half Maximum (FDHM) for all GFP oligomers and SDS-generated BBs completely supported previously observed significant differences. Solutions of GFP NPs were significantly more photostable than those of parental GFP-H6, which showed similar fluorescence decay rate as in SDS-generated BBs. An exception was R9-GFP-H6 BBs, which being still partially organized as 9 nm supramolecular structures did not completely reached the low photostability of the parental GFP-H6 (Figure 3B).

In a recent study [31], biophysical analyses of related protein NPs (in particular T22-DITOX-H6 and T22-GFP-H6, [32]) were suggestive of an enhanced structural stability of the oligomeric versions of such proteins, measured through resistance to thermal stress. We wondered if such robustness, presumably acquired through self-assembling, might be related to the photostability described in the present study. To address this question, we comparatively analyzed the X-ray radiation damage in SAXS on NP and BB forms of T22-GFP-H6 and A5-GFP-H6, the two proteins in which the disassembling protocol efficiently resulted in BBs. As observed (Figure 4), the assembled forms of both proteins were less vulnerable to damage produced by radical modification upon X-ray radiation over time than their unassembled counterparts. The detectable alteration of scattering intensities at low angles suggested the propensity of BBs to aggregate upon radiation damage, a common structural alteration catalyzed by amino acid modification though OH radicals [33]. Under the same radiation dose, the nanostructured GFP did not undergo observable macromolecular aggregation. In this sense, in our nanoparticle model, regions susceptible to radiation damage (with high content on Cys, Met, Phe, Tyr, Trp, Pro, His and Leu) are protected from solvent upon oligomerization (Supplementary Table 1). These data confirm that oligomeric forms of the protein are less sensitive to radiation stresses than the unassembled versions probably due to a reduced solvent exposure of

oxygen-reactive amino acids. Also in this context, the analysis of T22-GFP-H6 model (Figure 5) shows that the region of interaction between the monomers is very close and contain several amino acids described to be relevant in the generation of fluorescence. It is known that mutations in His 148, Met154, Val164, Ile167, Ser202, Thr 203 and Glu222 (marked as spheres in Figure 5) induce changes in GFP fluorescence[34-38]. Therefore, this fact points out that NP formation modifies the local environment of these amino acids that are important for the GFP chromophore formation, and therefore, self-assembling impacts on its stability under intense light irradiation.

4. DISCUSSION

Fluorescent proteins are exploited as molecular probes in bioimaging [1, 39] to report gene expression [40, 41], to dissect intracellular structures [42] and to determine intracellular localization and interactions at single molecule resolution [43, 44]. They are also promising to develop protein-based NPs for cell-targeted drug delivery in cancer, as they can be incorporated in the BBs for theranostic purposes [45]. In this context, NPs are usually functionalized with specific ligands of cell surface receptors for cell-targeted drug delivery [46-48]. However, the applicability of nanostructured vehicles as drug carriers has been so far compromised by an only limited success in reaching a good biodistribution of the drug. In most cases, only around 1 % of the administered material accumulates in the target site, while the rest distributes among healthy tissues [49, 50]. This landscape is not sufficient to enhance the therapeutic index of a free cytotoxic compound, such as those used in oncotherapy [51], and it is also insufficient to fulfill the requirements of a precise theranostic agent. In recent studies we have engineered a peptide-tagged recombinant GFP, that self-assembles as NPs of 12 nm [20, 22], to successfully deliver small molecular weight drugs [23] and human pro-apoptotic factors

[24] to metastatic cancer stem cells, in colorectal cancer animal models. The biodistribution of this material, as determined by fluorescence detection, is very selective and it fulfills the high standards required for both, drug delivery and imaging [10]. The protein, in an assembled and fluorescent form, is architectonically stable in circulation (Supplementary Figure 4) [11] and is only found inside target cells, either in the main tumor or in metastatic foci [10], but not in normal organs. Therefore, these nanostructured GFP show enormous potential in preclinical drug trials and in diagnostic formulations, both in cell culture and *in vivo* since targeted fluorescent NPs can be used to specifically deliver fluorescent proteins and conjugated drugs into target cells for precision imaging and theranosis. This fact prompted us to investigate the photostability of the protein fluorophore when GFP is organized as regular oligomeric NPs.

A self-assembling GFP, forming NPs of 12 nm in size, has been engineered to target $CXCR4^+$ tumor cells by the fusion to a CXCR4-binding peptide, namely T22. This nanostructured complex, biodistributes with exquisite precision upon intravenous injection in colorectal cancer mouse models, in which more than 85% of total detected fluorescence is accumulated specifically in tumoral tissues (including small metastatic foci) [10, 11]. This construct and derivatives are, therefore, extremely efficient for theranosis [23, 24]. Then, we wanted to determine their photostability compared to regular GFP versions to evaluate if the controlled oligomerization might have a positive effect in the robustness of fluorescence emission. We initially anticipated a decrease in the specific fluorescence, since in the NPs, the close GFP-GFP contacts [20] could cause substantial self-quenching. This has been recently demonstrated in GFP-loaded HBV-like NPs, where the distance between the internally localized GFP molecules strongly influenced their fluorescence signal [5]. However, in the current platform, the GFP fluorescence was not affected by self-assembling, as the engineered GFP variants were

equally emitting as NPs or BBs (Figure 1A). The fusion of a cationic peptide at the amino terminus of GFP had only a moderate impact on fluorescence, which was reduced up to about 70-90 % of the parental GFP-H6 (Figure 1A). In addition, the pH of the physiological media had no significant influence over both, the self-assembling and specific fluorescence of the protein samples, and they were also architectonically stable in human serum. This is important when protein NPs are designed for in-vivo imaging (Supplementary Figure 1 and 4). Importantly, photobleaching was dramatically reduced in oligomerized GFP compared to BB versions (Figure 2and 3), stressing the unanticipated positive impact of self-assembling in keeping the stability of the emitted fluorescence. Data also suggest that the observed fluorophore stability under laser irradiation is related to a globally enhanced protein structural stability, since the radiation damage over NP forms of GFP is clearly reduced over the parental unassembled GFP-H6 or the BB versions (Figure 4). In this context, both synchrotron X-ray beams and laser light induce photodamage to structurally similar fluorescent proteins resulting in loss of absorbance and fluorescence, a fact known to be influenced by the chromophore's local environment [52]. As an additional observation, the molecular weight of the target protein or protein complex influences the radiation damage in small-angle X-ray scattering with a protective effect [53]. In this context, recombinant GFP shows a tendency to uncontrolled multimerization and aggregation [54] and some oligomerizing GFP variants have shown affected fluorescence, photobleaching and blinking, depending on oligomer size [55]. It is well known that several residues involved in the chromophoric properties of GFP are close to the GFP dimer interface, which has been postulated as one of the contact sites between GFP BBs to form toroid NPs as those described here [20]. These observations and concepts would account for the particular differences observed in NPs performance and stability of fluorescent NPs *versus* GFP monomers or dimeric BBs under

electromagnetic radiation. Importantly, in the *in silico* models of T22-GFP-H6 NPs, that perfectly fit the morphometric nanoscale evaluation of the material [20, 22], the GFP residues involved in fluorescence participate or are in close proximity to the BB interfaces (Figure 5). This observation accounts for the enhanced stability of GFP promoted by its controlled oligomerization in form of NPs.

5. CONCLUSIONS

The administration of oligomeric GFP as cell-targeted NPs in cancer imaging, therapy and theranostic contexts, benefits from a multiplexed presentation of the tumoral cell ligand (here modelled by T22, A5 or R9), what favours cell internalization [56]. The nanoscale architecture of GFP also results in a highly selective biodistribution upon systemic administration, as it allows escaping from renal filtration [11] and the identification of small metastatic foci because of the longer circulation time [10]. We have here proved that in addition, the nanostructure of GFP NPs, easily regulatable by the manipulation of divalent cations [57], enhances the structural stability and photostability of the system. Therefore, being photobleaching a major obstacle in the application of GFP and other fluorescent proteins in imaging and theranosis, the controlled oligomerization of fluorescent proteins appears as a powerful method to enhance their photostability for their use in precision imaging and therapy.

AUTHOR INFORMATION

Corresponding Authors

* Ugutz Unzueta: UUnzueta@santpau.cat

* Antonio Villaverde: antoni.villaverde@uab.es

* Esther Vazquez: esther.vazquez@uab.es

Present Addresses

$ Institute for Research in Biomedicine (IRB Barcelona), The Barcelona Institute of Science and Technology, Barcelona 08028, Spain.

Author Contributions

The manuscript was written through contributions of all authors. All authors have given approval to the final version of the manuscript. ‡These authors contributed equally.

ACKNOWLEDGMENTS.

This study has been funded by the Agencia Estatal de Investigación (AEI) and Fondo Europeo de Desarrollo Regional (FEDER) (grant BIO2016-76063-R, AEI/FEDER, UE), AGAUR (2017SGR-229) and CIBER-BBN (project VENOM4CANCER) granted to AV, ISCIII (PI15/00272 co-founding FEDER) granted to EV and CIBER-BBN (project NANOSCAPE) granted to UUE. Protein production and DLS measurements have been partially performed by the ICTS “NANBIOSIS”, more specifically protein production by the Protein Production Platform of CIBER-BBN/IBB (http://www.nanbiosis.es/unit/u1-protein-production-platform-ppp/) and nanoparticle size analysis by the Biomaterial Processing and Nanostructuring Unit (http://www.nanbiosis.es/portfolio/u6-biomaterial-

processing-and-nanostructuring-unit/). We are indebted to the Servei de Microscòpia of the UAB for excellent technical service. UU is supported by PERIS program from the health department of la Generalitat de Cataluña. R.B. was supported by research grant SAF2017-8819-C3 from the Spanish Ministry of Science Innovation and Universities. AV received an ICREA ACADEMIA award. EV, RM and AV are co-founders of NANOLIGENT, devoted to develop antitumoral drugs based on proteins.

ABBREVIATIONS

NPs, Nanoparticles; BBs, Building Blocks; FDHM, Full Duration at Half Maximum; DLS, Dynamic Light Scattering; SAXS, Small Angle X-ray Scattering; SDS, Sodium Dodecyl Sulphate.

FIGURES:

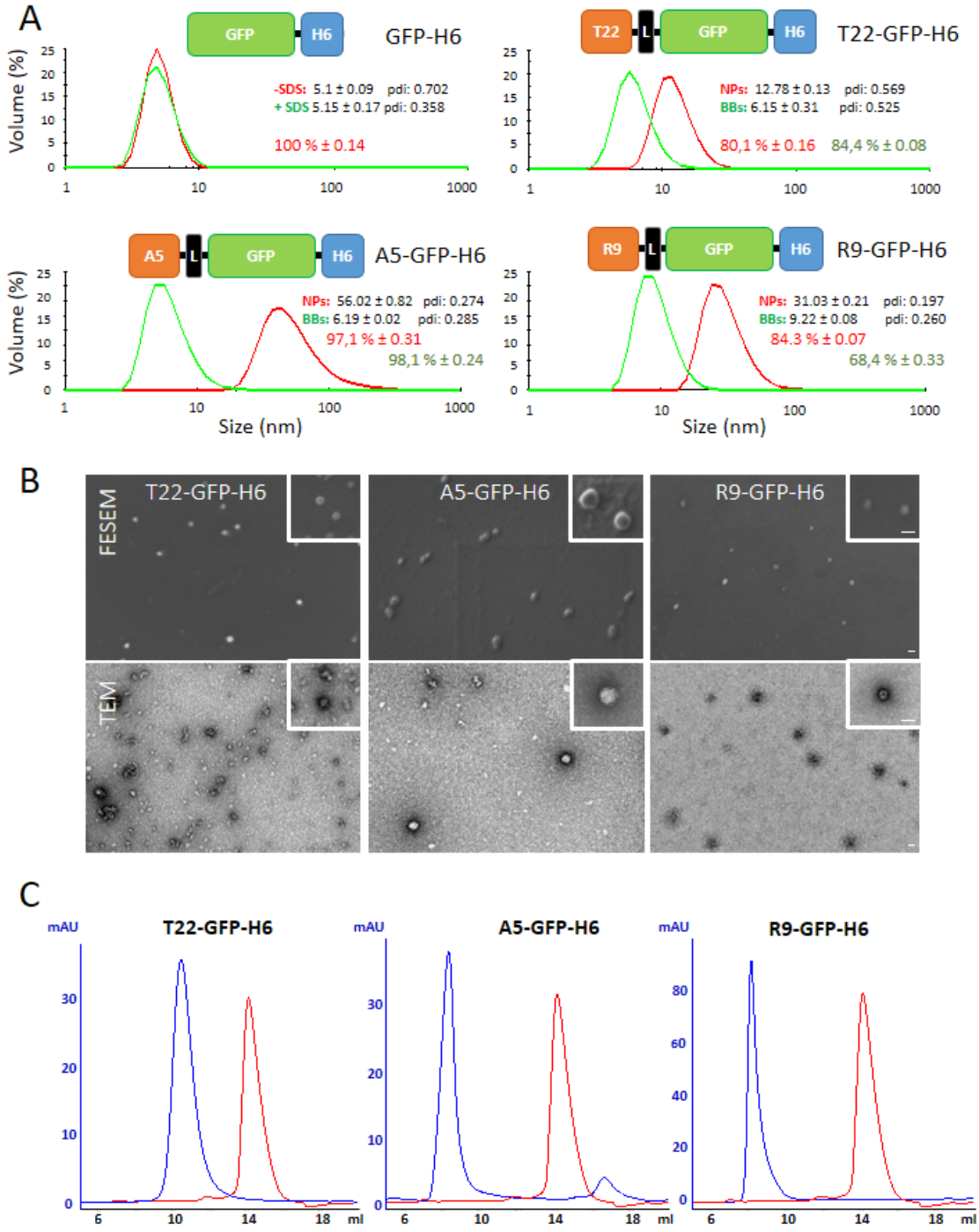

Figure 1. Structure and architecture of protein NPs A) Modular organization and hydrodynamic size of T22-GFP-H6, A5-GFP-H6 and R9-GFP-H6 self-assembled protein

nanoparticles (NPs) measured by DLS. SDS-disassembled BBs are also indicated. The parental GFP-H6 protein used as a control has been also analyzed in presence and absence of SDS. All data are expressed as $\overline{x} \pm$ SE, and pdi indicates the polydispersion index. Relative sizes of boxes are only indicative. Precise information about the constructs can be found elsewhere [10, 21, 58] and supplementary data. Average fluorescence emission relative to GFP-H6 (in %) is indicated for each protein sample, in red or green typography. B) Electron microscopy (FESEM-top and TEM-bottom) images of purified T22-GFP-H6, A5-GFP-H6 and R9-GFP-H6 nanoparticles showing their cyclic nanostructure. Two magnifications are presented (see insets), equivalent in all images. Scale bars indicate 25 nm. C) Size exclusion chromatography profiles of T22-GFP-H6, A5-GFP-H6 and R9-GFP-H6 NPs (in blue). Parental GFP-H6 protein profile is indicated (in red) as a reference to identify peaks corresponding to non-assembled BBs.

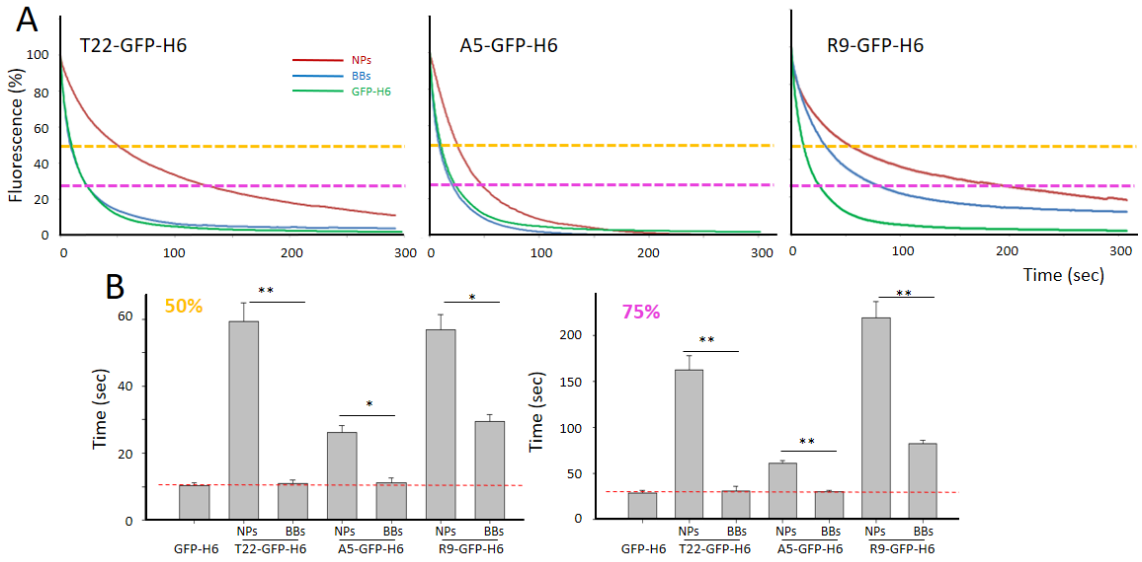

Figure 2. Protein nanoparticles photostability A) Photobleaching curves for T22-GFP-H6, A5-GFP-H6 and R9-GFP-H6 NPs and BBs. GFP-H6 is added as a control in all the measures. Data was recorded by confocal laser microscopy upon excitation at 488 nm by a 20 mW argon laser during subsequent frames. Orange dashed lines indicate 50 % of photobleaching while pink dashed lines indicate 75 % of photobleaching. The initial intensities of fluorescence were assumed as 100 %. B) Graphical quantification of 50 % (left) and 75 % (right) photobleaching times for different protein samples. Red dashed line indicates photobleaching times corresponding to control GFP-H6 protein. * indicates $p<0.01$ and ** indicates $p<0.001$.

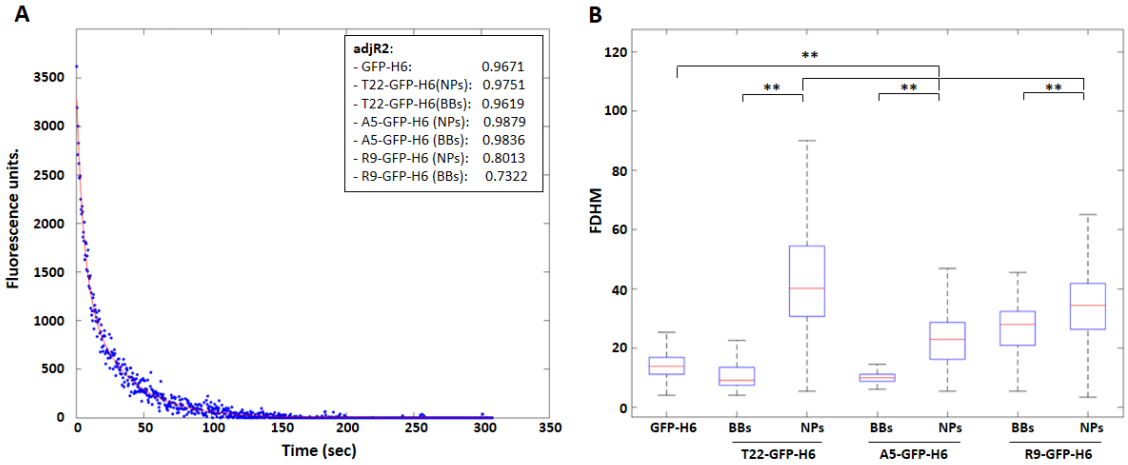

Figure 3: Nanoparticles fluorescence decay analysis. A) Double exponential fitting of parental GFP-H6 fluorescence decay analyzed at pixel level. Average adjusted R-squared for all protein samples are indicated in the inset as goodness of fit parameter. B) Graphical quantification of Full Duration at Half Maximum (FDHM) for different protein samples analyzed at pixel level. ** indicates $p<0.001$.

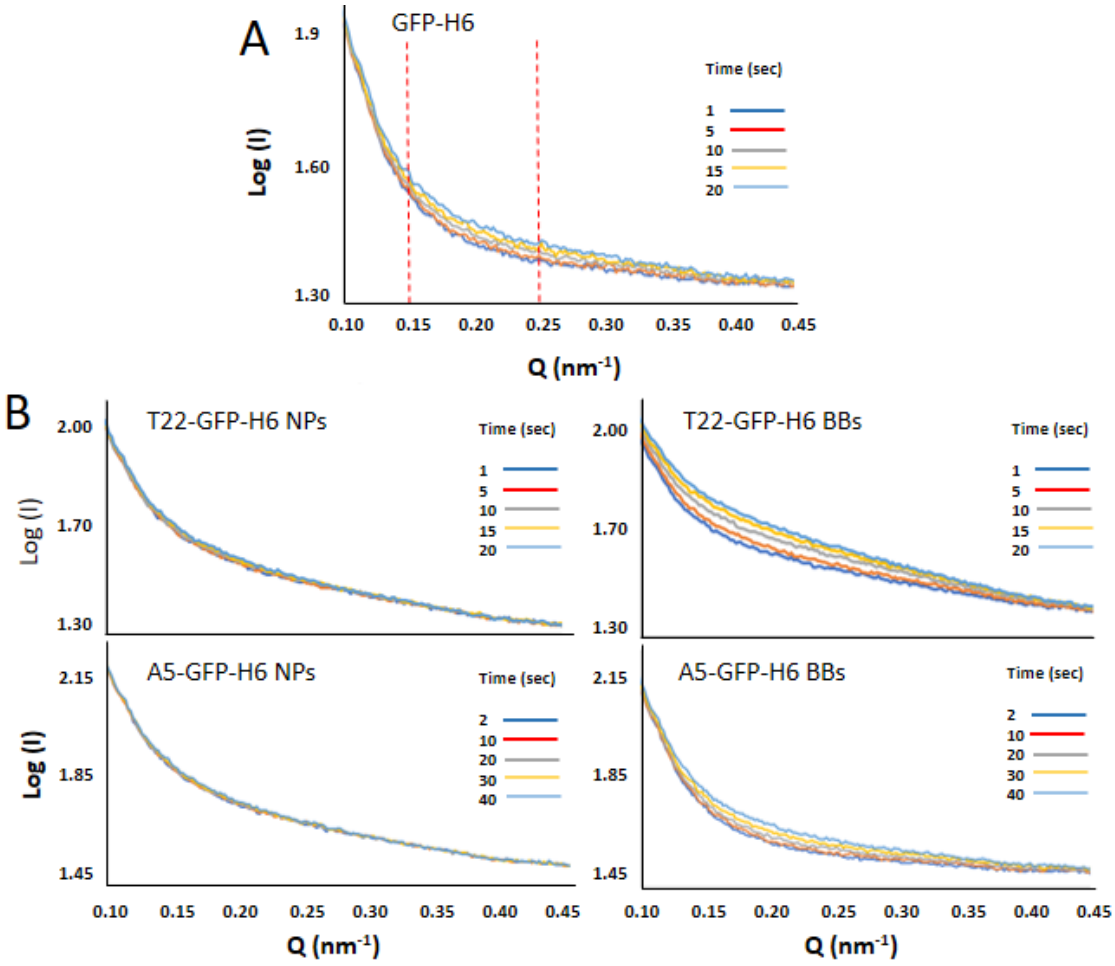

Figure 4. Structural stability of protein nanoparticles. Radiation damage over (A) control GFP-H6 protein or over (B) T22-GFP-H6 and A5-GFP-H6 protein nanoparticles (NPs) and building blocks (BBs) measured by progressive changes (indicated between red dashed line) observed over Small Angle X-ray scattering curves upon exposition at 12.4 keV light source during subsequent frames.

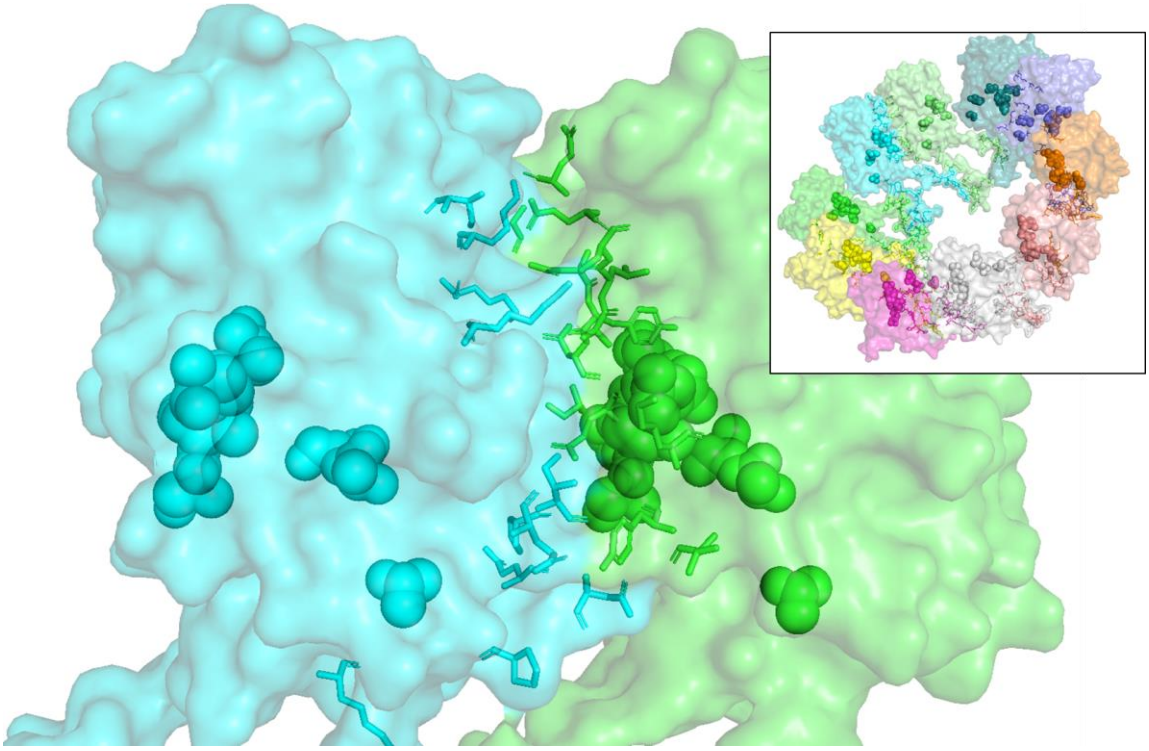

Figure 5. BB interfaces in T22GFP-H6 NPs Two contiguous T22-GFP-H6 monomers of T22-GFP-H6 NPs are depicted in transparent surface representation of an *in silico* modelled NP. Interface residues (those supporting cross-molecular BB contacts) are presented as sticks, and residues known to affect the fluorescence of the protein are shown as spheres. Note the interaction and global proximity between them. In the inset, an overview of the full NP.

Table 1. Comparative photostability (shown as enhancement factor) of engineered GFP proteins.

	GFP-H6		BB	
	BB[a]	NP	BB	NP
T22-GFP-H6	1.06	7.72	-	5.42
A5-GFP-H6	1.08	2.54	-	2.34
R9-GFP-H6	2.85	5.49	-	1.93

[a] Fold reduction of 50 % photobleaching in NPs compared to either the parental GFP-H6 (GFP-H6 column) or to the BB version of each protein (BB column) upon SDS-mediated disassembly.

References

[1] Rodriguez EA, Campbell RE, Lin JY, Lin MZ, Miyawaki A, Palmer AE, Shu X, Zhang J, Tsien Ry. The Growing and Glowing Toolbox of Fluorescent and Photoactive Proteins. Trends in biochemical sciences 2017;42:111-29.

[2] Hoffman RM. Application of GFP imaging in cancer. Laboratory investigation; a journal of technical methods and pathology 2015;95:432-52.

[3] Ntziachristos V, Yoo JS, van Dam GM. Current concepts and future perspectives on surgical optical imaging in cancer. Journal of biomedical optics 2010;15:066024.

[4] Hoffman RM. The multiple uses of fluorescent proteins to visualize cancer in vivo. Nature reviews Cancer 2005;5:796-806.

[5] Kim SE, Jo SD, Kwon KC, Won YY, Lee J. Genetic Assembly of Double-Layered Fluorescent Protein Nanoparticles for Cancer Targeting and Imaging. Advanced science 2017;4:1600471.

[6] Yano S, Takehara K, Miwa S, Kishimoto H, Tazawa H, Urata Y, Kagawa S, Bouvet M, Fujiwara T, Hoffman R. Fluorescence-guided surgery of a highly-metastatic variant of human triple-negative breast cancer targeted with a cancer-specific GFP adenovirus prevents recurrence. Oncotarget 2016;7:75635-47.

[7] Metildi CA, Kaushal S, Snyder CS, Hoffman RM, Bouvet M. Fluorescence-guided surgery of human colon cancer increases complete resection resulting in cures in an orthotopic nude mouse model. The Journal of surgical research 2013;179:87-93.

[8] Miyamoto S, Sperry S, Yamashita T, Reddy NP, O'Malley BW, Jr., Li D. Molecular imaging assisted surgery improves survival in a murine head and neck cancer model. Int J Cancer 2012;131:1235-42.

[9] Lippincott-Schwartz J, Patterson GH. Development and use of fluorescent protein markers in living cells. Science 2003;300:87-91.

[10] Unzueta U, Cespedes MV, Ferrer-Miralles N, Casanova I, Cedano J, Corchero JL, Domingo-Espín J, Villaverde A, Mangues R, Vazquez E. Intracellular CXCR4(+) cell targeting with T22-empowered protein-only nanoparticles. International journal of nanomedicine 2012;7:4533-44.

[11] Cespedes MV, Unzueta U, Tatkiewicz W, Sanchez-Chardi A, Conchillo-Sole O, Alamo P, Xu Z, Casanova I, Corchero JL, Pesarrodona M, Cedano J, Daura X, Ratera I, Veciana J, Ferrer-Miralles N, Vazquez E, Villaverde A, Mangues R. In vivo architectonic stability of fully de novo designed protein-only nanoparticles. ACS nano 2014;8:4166-76.

[12] Cespedes MV, Unzueta U, Alamo P, Gallardo A, Sala R, Casanova I, Pavon MA, Mangues MA, Trias M, Lopez-Pousa A, Villaverde A, Vazquez E, Mangues R. Cancer-specific uptake of a liganded protein nanocarrier targeting aggressive CXCR4+ colorectal cancer models. Nanomedicine : nanotechnology, biology, and medicine 2016;12:1987-96.

[13] Mamontova AV, Grigoryev AP, Tsarkova AS, Bogdanov KALAM. Struggle for Photostability: Bleaching Mechanisms of Fluorescent Proteins. Russ J Bioorg Chem+ 2017;43:9.

[14] Zhang C, Konopka JB. A photostable green fluorescent protein variant for analysis of protein localization in Candida albicans. Eukaryotic cell 2010;9:224-6.

[15] Bajar BT, Wang ES, Lam AJ, Kim BB, Jacobs CL, Howe ES, Davidson MW, Lin MZ, Chu J. Improving brightness and photostability of green and red fluorescent proteins for live cell imaging and FRET reporting. Scientific reports 2016;6:20889.

[16] Bogdanov AM, Bogdanova EA, Chudakov DM, Gorodnicheva TV, Lukyanov S, Lukyanov KA. Cell culture medium affects GFP photostability: a solution. Nature methods 2009;6:859-60.

[17] Kiss C, Temirov J, Chasteen L, Waldo GS, Bradbury AR. Directed evolution of an extremely stable fluorescent protein. Protein engineering, design & selection : PEDS 2009;22:313-23.

[18] Fu Y, Zhang J, Lakowicz JR. Metal-enhanced fluorescence of single green fluorescent protein (GFP). Biochemical and biophysical research communications 2008;376:712-7.

[19] Mamontova AV, Bogdanov AM, Lukyanov KA. Influence of cell growth conditions and medium composition on EGFP photostability in live cells. BioTechniques 2015;58:258-61.

[20] Rueda F, Cespedes MV, Conchillo-Sole O, Sanchez-Chardi A, Seras-Franzoso J, Cubarsi R, Gallardo A, Pesarrodona M, Ferrer-Miralles N, Daura X, Vazquez E, Garcia-Fruitos E, Mangues R, Unzueta U, Villaverde A. Bottom-Up Instructive Quality Control in the Biofabrication of Smart Protein Materials. Advanced materials 2015;27:7816-22.

[21] de Pinho Favaro MT, Serna N, Sanchez-Garcia L, Cubarsi R, Roldan M, Sanchez-Chardi A, Unzueta U, Mangues R, Ferrer-Miralles N, Azzoni AR, Vazquez E, Villaverde A. Switching cell penetrating and CXCR4-binding activities of nanoscale-organized arginine-rich peptides. Nanomedicine : nanotechnology, biology, and medicine 2018.

[22] Pesarrodona M, Crosas E, Cubarsi R, Sanchez-Chardi A, Saccardo P, Unzueta U, Rueda F, Sanchez-Garcia L, Serna N, Mangues R, Ferrer-Miralles N, Vazquez E, Villaverde A. Intrinsic functional and architectonic heterogeneity of tumor-targeted protein nanoparticles. Nanoscale 2017;9:6427-35.

[23] Cespedes MV, Unzueta U, Avino A, Gallardo A, Alamo P, Sala R, Sanchez-Chardi A, Casanova I, Mangues MA, Lopez-Pousa A, Eritja R, Villaverde A, Vazquez E, Mangues R. Selective depletion of metastatic stem cells as therapy for human colorectal cancer. EMBO molecular medicine 2018.

[24] Serna NC, M; Sánchez-García, L; Unzueta, U; Sala, R; Sánchez-Chardi, A; Cortés, F; Ferrer-Miralles, N; Mangues, R; Vázquez, E; Villaverde, A. Peptide-

Based Nanostructured Materials with Intrinsic Proapoptotic Activities in CXCR4+ Solid Tumors. Advanced Functional Materials 2017;27:1700919.

[25] Pesarrodona M, Ferrer-Miralles N, Unzueta U, Gener P, Tatkiewicz W, Abasolo I, Ratera I, Veciana J, Schwartz S Jr, Villaverde A, Vazquez E. Intracellular targeting of CD44+ cells with self-assembling, protein only nanoparticles. International journal of pharmaceutics 2014;473:286-95.

[26] Cano-Garrido O, Garcia-Fruitos E, Villaverde A, Sanchez-Chardi A. Improving Biomaterials Imaging for Nanotechnology: Rapid Methods for Protein Localization at Ultrastructural Level. Biotechnol J 2018;13:e1700388.

[27] de Vries SJ, van Dijk AD, Krzeminski M, van Dijk M, Thureau A, Hsu V, Wassenaar T, Bonvin AM. HADDOCK versus HADDOCK: new features and performance of HADDOCK2.0 on the CAPRI targets. Proteins 2007;69:726-33.

[28] Thornton SJHJM. "NACCESS", Computer Biochemistry and Molecular Biology, University College London,1993.

[29] Gautier I, Tramier M, Durieux C, Coppey J, Pansu RB, Nicolas JC, Kemnitz K, Coppey-Moisan M. Homo-FRET microscopy in living cells to measure monomer-dimer transition of GFP-tagged proteins. Biophys J 2001;80:3000-8.

[30] Campbell RE, Tour O, Palmer AE, Steinbach PA, Baird GS, Zacharias DA, Tsien RY. A monomeric red fluorescent protein. Proceedings of the National Academy of Sciences of the United States of America 2002;99:7877-82.

[31] Sanchez JM, Sanchez-Garcia L, Pesarrodona M, Serna N, Sanchez-Chardi A, Unzueta U, Mangues R, Vazquez E, Villaverde A. Conformational Conversion during Controlled Oligomerization into Nonamylogenic Protein Nanoparticles. Biomacromolecules 2018;19:3788-97.

[32] Sanchez-Garcia L, Serna N, Alamo P, Sala R, Cespedes MV, Roldan M, Sánchez-Chardi A, Unzueta U, Casanova I, Mangues R, Vázquez E, Villaverde A. Self-assembling toxin-based nanoparticles as self-delivered antitumoral drugs.

Journal of controlled release: official journal of the Controlled Release Society 2018;274:81-92.

[33] Maleknia SD, Ralston CY, Brenowitz MD, Downard KM, Chance MR. Determination of macromolecular folding and structure by synchrotron x-ray radiolysis techniques. Analytical biochemistry 2001;289:103-15.

[34] Campanini B, Pioselli B, Raboni S, Felici P, Giordano I, D'Alfonso L, Collini M, Chirico G, Bettati S. Role of histidine 148 in stability and dynamics of a highly fluorescent GFP variant. Biochimica et biophysica acta 2013;1834:770-9.

[35] Natarajan A, Subramanian S, Srienc F. Comparison of mutant forms of the green fluorescent protein as expression markers in Chinese hamster ovary (CHO) and Saccharomyces cerevisiae cells. Journal of biotechnology 1998;62:29-45.

[36] Liu SS, Wei X, Dong X, Xu L, Liu J, Jiang B. Structural plasticity of green fluorescent protein to amino acid deletions and fluorescence rescue by folding-enhancing mutations. BMC Biochem 2015;16:17.

[37] Heim R, Prasher DC, Tsien RY. Wavelength mutations and posttranslational autoxidation of green fluorescent protein. Proceedings of the National Academy of Sciences of the United States of America 1994;91:12501-4.

[38] Jung G, Wiehler J, Zumbusch A. The photophysics of green fluorescent protein: influence of the key amino acids at positions 65, 203, and 222. Biophys J 2005;88:1932-47.

[39] Miyawaki A, Niino Y. Molecular spies for bioimaging--fluorescent protein-based probes. Molecular cell 2015;58:632-43.

[40] Yang M, Baranov E, Moossa AR, Penman S, Hoffman RM. Visualizing gene expression by whole-body fluorescence imaging. Proceedings of the National Academy of Sciences of the United States of America 2000;97:12278-82.

[41] Contag CH, Bachmann MH. Advances in in vivo bioluminescence imaging of gene expression. Annual review of biomedical engineering 2002;4:235-60.

[42] Sahl SJ, Hell SW, Jakobs S. Fluorescence nanoscopy in cell biology. Nature reviews Molecular cell biology 2017;18:685-701.

[43] Duwe S, De Zitter E, Gielen V, Moeyaert B, Vandenberg W, Grotjohann T, Clays K, Jakobs S, Van Meervelt, Dedecker P. Expression-Enhanced Fluorescent Proteins Based on Enhanced Green Fluorescent Protein for Super-resolution Microscopy. ACS nano 2015;9:9528-41.

[44] Shashkova S, Leake MC. Single-molecule fluorescence microscopy review: shedding new light on old problems. Bioscience reports 2017;37.

[45] Vazquez E, Mangues R, Villaverde A. Functional recruitment for drug delivery through protein-based nanotechnologies. Nanomedicine 2016;11:1333-6.

[46] Yao VJ, D'Angelo S, Butler KS, Theron C, Smith TL, Marchio S, Gelovani JG, Sidman RL, Dobroff AS, Brinker CJ, Bradbury ARM, Arap W, Pasqualini R.. Ligand-targeted theranostic nanomedicines against cancer. Journal of controlled release : official journal of the Controlled Release Society 2016;240:267-86.

[47] Caster JM, Patel AN, Zhang T, Wang A. Investigational nanomedicines in 2016: a review of nanotherapeutics currently undergoing clinical trials. Wiley interdisciplinary reviews Nanomedicine and nanobiotechnology 2017;9.

[48] David A. Peptide ligand-modified nanomedicines for targeting cells at the tumor microenvironment. Advanced drug delivery reviews 2017;119:120-42.

[49] Duncan R, Gaspar R. Nanomedicine(s) under the microscope. Molecular pharmaceutics 2011;8:2101-41.

[50] Stefan Wilhelm AJT, Qin Dai, Seiichi Ohta, Julie Audet, Harold F. Dvorak & Warren C. W. Chan. Analysis of nanoparticle delivery to tumours. Nature Reviews Materials 2016;1.

[51] Serna N, Sanchez-Garcia L, Unzueta U, Diaz R, Vazquez E, Mangues R, Villaverde A. Protein-Based Therapeutic Killing for Cancer Therapies. Trends in biotechnology 2018;36:318-35.

[52] Adam V, Carpentier P, Violot S, Lelimousin M, Darnault C, Nienhaus GU, Bourgeois D. Structural basis of X-ray-induced transient photobleaching in a photoactivatable green fluorescent protein. Journal of the American Chemical Society 2009;131:18063-5.

[53] Hopkins JB, Thorne RE. Quantifying radiation damage in biomolecular small-angle X-ray scattering. Journal of applied crystallography 2016;49:880-90.

[54] Schrödel A, de Marco A. Characterization of the aggregates formed during recombinant protein expression in bacteria. BMc Biochemistry 2005;6:10.

[55] Vamosi G, Mucke N, Muller G, Krieger JW, Curth U, Langowski J, Tóth K. EGFP oligomers as natural fluorescence and hydrodynamic standards. Scientific reports 2016;6:33022.

[56] Unzueta U, Cespedes MV, Vazquez E, Ferrer-Miralles N, Mangues R, Villaverde A. Towards protein-based viral mimetics for cancer therapies. Trends in biotechnology 2015;33:253-8.

[57] Lopez-Laguna H, Unzueta U, Conchillo-Sole O, Sanchez-Chardi A, Pesarrodona M, Cano-Garrido O, Voltà E, Sánchez-García L, Serna N, Saccardo P, Mangues R, Villaverde A, Vazquez E. Assembly of histidine-rich protein materials controlled through divalent cations. Acta biomaterialia 2018.

[58] Pesarrodona M, Fernandez Y, Foradada L, Sanchez-Chardi A, Conchillo-Sole O, Unzueta U, Xu Z, Roldán M, Villegas S, Ferrer-Miralles N, Schwartz SJr, Rinas U, Daura X, Abasolo I, Vazquez E, Villaverde A. Conformational and functional variants of CD44-targeted protein nanoparticles bio-produced in bacteria. Biofabrication 2016;8:025001.